Global Change Biology (2008) **14**, 1690–1702, doi: 10.1111/j.1365-2486.2008.01589.x

Closing the carbon budget of estuarine wetlands with tower-based measurements and MODIS time series

YANER YAN*, BIN ZHAO*, JIQUAN CHEN†, HAIQIANG GUO*, YONGJIAN GU*, QIANHONG WU* and BO LI*

*Coastal Ecosystems Research Station of the Yangtze River Estuary, Ministry of Education Key Laboratory for Biodiversity Science and Ecological Engineering, Institute of Biodiversity Science, Fudan University, Shanghai 200433, China, †Department of Environmental Sciences, University of Toledo, Toledo, OH, USA

Abstract

Compared to other ecosystems, estuarine ecosystems have distinct carbon flux dynamics – the lateral carbon flux incurred by tidal activities, and methane generation under the anaerobic conditions of wetland soils. The conventional estimation of gross primary production (GPP) based on the light use efficiency (LUE) model used for non-wetland terrestrial ecosystems, therefore, cannot be applied directly to estuarine wetland ecosystems. In this paper, we estimated the 2005's annual carbon budget of an estuarine wetland on Chongming Island, Shanghai, and partitioned the losses of carbon due to lateral tidal dynamics and anaerobic methane production using an innovative technique. The average GPP calculated from eddy covariance between March and November was 261.79 μmol m^{-2} day^{-1}, whereas that from the LUE model was 58.84 μmol m^{-2} day^{-1}. The correlation coefficient between GPP simulated from the LUE model and that calculated from flux tower data was low in the growing season ($R^2 = 0.55$). We hypothesized that tidal activities and uncounted methane release were responsible for the difference, which can be predicted from measurements of remote sensing products such as land surface water index (LSWI), evapotranspiration (ET), and tide height (TH). We developed an integrated GPP model by combining the LUE model and an autoregression model to estimate carbon budget. The average GPP from the modified model increased to 263.38 μmol m^{-2} day^{-1}, and R^2 for the correlation between the simulated and calculated data increased to 0.88, demonstrating the potential of our technique for GPP estimation and quantification of seasonal variation in estuarine ecosystems. The approach developed in this study has great potential for correcting unavoidable errors when estimating carbon budget of coastal wetlands. Furthermore, global warming is expected to accelerate sea level rise, which may enhance the effect of tidal activities and increase the difficulty in estimating coastal carbon budgets using conventional methods.

Keywords: CH_4, CO_2, eddy covariance, estuarine wetland, lateral carbon flux, MODIS

Received 18 July 2007; revised version received 25 November 2007 and accepted 5 December 2007

Introduction

A recent report by IPCC (http://ipcc-wg1.ucar.edu/wg1/wg1-report.html) state that coastal wetlands are highly sensitive to climate change, and one of the greatest challenges in understanding the functioning of the estuarine ecosystems is how to accurately estimate the carbon budget. Accurate estimates of carbon dioxide and water vapor exchange between ecosystems and atmosphere are extremely valuable both for global climate change studies and for management of water and ecosystems (Houborg & Soegaard, 2004). The eddy covariance (EC) technique provides direct measurements of net exchange of CO_2, water, and energy between ecosystems and the atmosphere, allowing us to examine changes and mechanistic regulations at multiple temporal and spatial scales (Baldocchi *et al*., 2001; Chen & Chen, 2004; Leuning *et al*., 2005). However, scaling up from the ecosystem level (i.e. based on EC towers) to broader spatial scales (i.e. landscape and region) remains challenging because of (1) interactions

Correspondence: Bin Zhao, tel. + 86 21 65642263 2, fax + 86 21 6564246, e-mail: zhaobin@fudan.edu.cn

among ecosystems (Chen *et al*., 2006) and (2) spatial complexity in landform, soil, and microclimate that prevents use of the EC method (Paw U *et al*., 2000; Scanlon & Albertson, 2003; Chen & Chen, 2004). Remote sensing technology, meanwhile, can be an effective tool for regional studies because it provides consistent and systematic observations of land surface properties. Recent success in modeling gross primary production (GPP) (Running *et al*., 1999) and evapotranspiration (ET) (Boegh & Soegaard, 2004; Houborg & Soegaard, 2004; Nagler *et al*., 2005a, b) indicates that remote sensing technology may have potential for studying carbon and water fluxes. Among the numerous challenges inherent in applying this approach, accuracy assessment and necessary validation with ground measurements are critical – suggesting that an approach that combines EC measurements with remotely sensed data could provide opportunities for regional studies of ecosystem processes (Reich *et al*., 1999; Turner *et al*., 2003a; Nagler *et al*., 2005b; Heinsch *et al*., 2006).

A limited number of studies integrating flux tower measurements and remote sensing products have been conducted over the recent years, with emphasis on validation and scaling-up in forests, agricultural grasslands, and arctic tundra landscapes (Turner *et al*., 2005, 2006; Xiao *et al*., 2005; Heinsch *et al*., 2006). Very few studies, however, have been conducted in wetland-dominated landscapes. We have not found any relevant published studies on estuarine wetlands, regardless of their importance in balancing the global carbon budget (Martinelli *et al*., 1991) and conserving biological diversity (i.e. species hot spots). Our study is among the first to estimate carbon and water fluxes of estuarine wetlands using EC measurements and remote sensing products.

Physical models of estuarine carbon balance

Estuarine wetlands are characterized by complex interactions between vegetation type, strong and frequent surface water movements (e.g. tides), and pore water movement (Hughes *et al*., 1998). Many factors (e.g. topography, the vegetation heterogeneity, the temporal distribution of rainfall, seasonal variations of ET, and tidal activity) can play critical roles in influencing the hydrology of wetlands (Hughes *et al*., 1998) and, consequently, other ecosystem properties such as carbon fluxes. In addition to the vertical carbon exchange between ecosystem and atmosphere, lateral carbon exchange between the wetland and offshore water through tidal activity and CH_4 release from anaerobic soil also need to be accounted for when net ecosystem exchange (NEE) of carbon, water, and energy is quantified (Teal, 1962; Odum, 1968, 2000; Drake *et al*., 1996). For example, Winter *et al*. (1996) used concentrations of dissolved inorganic carbon, dissolved organic carbon, and particulate organic carbon to quantify the total carbon exported from the estuary to the ocean and found that 4755 tons yr^{-1} were carried to the ocean. Bange (2006) studied the distributions of N_2O and CH_4 in European coastal areas and reported that average CH_4 emissions were 0.21 and 0.35 Tg C yr^{-1} for European shelves and estuaries.

Conceptually, the gross ecosystem exchange (GEE) of carbon in estuarine wetland ecosystems can be expressed as

$$\mathrm{GEE} = \mathrm{GPP} + F_{\mathrm{lateral}} + F_{\mathrm{CH_4}} + F_{\mathrm{other}}, \quad (1)$$

where F_{lateral} is the lateral exchange of C between the wetland and offshore water through diffusion and tidal movement, $F_{\mathrm{CH_4}}$ is the amount of CH_4 released into the air, and F_{other} is other uncounted C exchange. In practice, GEE may be calculated from NEE measurements obtained from the EC tower, while GPP may be estimated from remote sensing products such as MODIS (Moderate Resolution Imaging Spectrometer). The lateral flux, methane flux, and other flux terms in Eqn (1) cannot be modeled with high confidence using remote sensing products. Heinsch *et al*. (2006) reported that GEE estimates from EC towers matched GPP estimates from MODIS very well, yet no similar efforts have been made for wetland systems.

MODIS-based GPP/NPP estimations

GPP is conventionally estimated based on light use efficiency (LUE) through remote sensing and modeling by deriving important vegetation measurements such as vegetation indices, the leaf area index (LAI), and LUE (Waring *et al*., 1995; Turner *et al*., 2003a, b; Heinsch *et al*., 2006; Xiao, 2006). In this study, we used the MODIS products to predict landscape-level GPP. The sensor on board the NASA Terra satellite has 36 spectral bands. Seven spectral bands, blue (459–479 nm), green (545–565 nm), red (620–670 nm), near infrared (841–875 nm, 1230–1250 nm), and shortwave infrared (1628–1652 nm, 2105–2155 nm) are primarily designed for the study of vegetation and land surface. Since the launch of MODIS in March 2000, it has been used widely in estimation and evaluation of GPP and NPP. For example, Gebremichael & Barros (2006) evaluated MODIS GPP in the tropical monsoon region in Marsyandi and Sonora and found a positive bias for the mixed forest biome in the Marsyandi basin and a negative bias for open shrub lands in the Sonora basin. Xiao *et al*. (2004a, b) used MODIS data to partition chlorophyll and nonphotosynthetically active vegetation (NPV) within a canopy and to develop a highly accurate ($R^2 = 0.89$–0.94) vege-

tation photosynthesis model (VPM) to estimate GPP based on the LUE model (Duan *et al*., 2005; Xiao *et al*., 2005; Li *et al*., 2006). Their work successfully demonstrated the potential of VPM for GPP estimation in forest and grassland ecosystems.

Although satellite-based GPP estimations have been tested widely for acceptable accuracy, we are cautious about replicating the process in estuarine or tide-influenced coastal wetlands because no model has considered lateral carbon exchange between sea and land, and few have included CH_4 flux, yet these are important processes in coastal wetlands. Our study objectives were threefold: (1) to examine biophysical performance of vegetation in relation to seasonal dynamics of CO_2 flux in an estuarine wetland by coupling MODIS signature and flux measurements of C and water, (2) to evaluate the feasibility and dependability of the MODIS-based model for estimating GPP in estuarine wetlands, and (3) to develop an integrated model combining the MODIS-based model and empirical models developed to account for lateral carbon exchange and CH_4 release.

Materials and methods

Study sites

Our study area was located on the east shore of Chongming Island, known as Dongtan, Shanghai – the largest wetland (ca. 230 km^2) in the Yangtze River estuary (Fig. 1). Annual precipitation of 1000.4 mm and a mean temperature of 15.3 °C characterize the climate. Tidal movement at Dongtan is regular and semidiurnal, with maximum and average tide heights (TH) of 4.62–5.95 m and 1.96–3.08 m, respectively (Chen & Chen, 2004). Three eddy flux towers were installed in August 2004 in different vegetation types to provide continuous records of NEE of carbon and water for understanding the C flux and budget of the estuarine wetlands in the Yangtze Delta and for validation of remote sensing models. The towers were installed on higher tideland near the dike (D: 31°31.000′N, 121°57.643′E), on lower tideland near the sea (S: 31°31.013′N, 121°58.297′E), and on mid-level tideland (M: 31°35.079′N, 121°54.207′E) (Fig. 1). The three sites had contrasting plant species, biomass, and microclimate (Table 1). We ensured a minimum of 100 sensor heights (i.e. 500 m, as 3-D sonic anemometers were installed at about 5 m above the vegetation) of fetch in all directions around each flux tower. The flux data were recorded on data loggers at 10 Hz, and 30 min averages were calculated during the growing season for later analyses. Data from March to November of 2005 were included in this study.

Eddy covariance data analysis

Daily GPP values during the study period were calculated from half-hourly fluxes of NEE and night-time ecosystem respiration at each site (Fig. 2). Major data

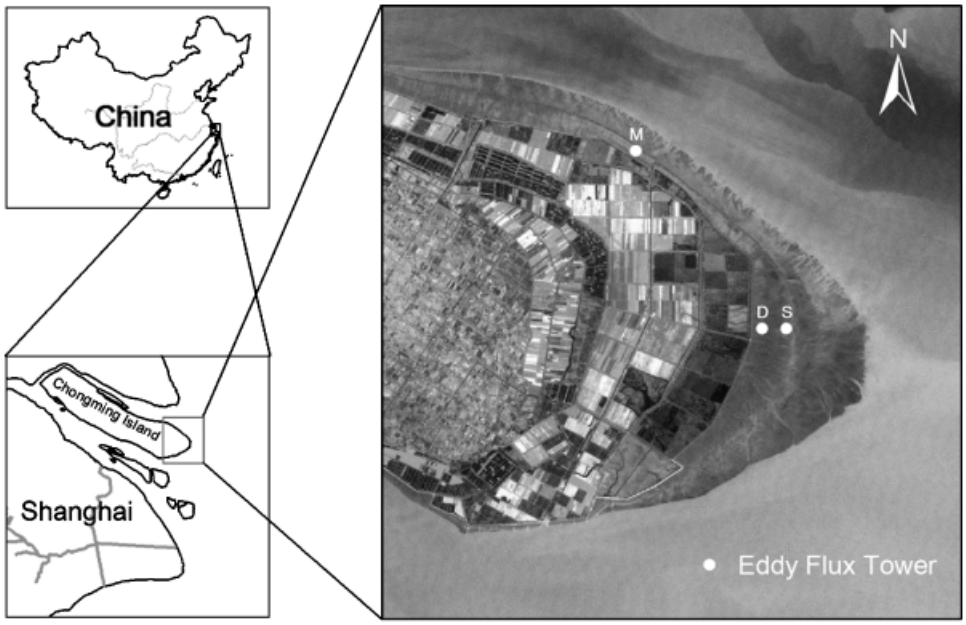

Fig. 1 Locations of study sites in estuarine wetlands in eastern Chongming Island (i.e. Dongtan), Shanghai, China. Three eddy covariance flux towers were installed in 2004 at a low intertidal area near the sea (S), a relatively higher-elevation area near the dike (D), and a mid-level Site (M) between S and D.

quality control included spike removal, two-axis rotation, and WPL correction (Leuning & Moncrieff, 1990). Several criteria were adopted to identify invalid data for removal, including (1) outliers that could not be explained by any known physical mechanisms, (2) data recorded during rainfall events, and (3) night-time NEE (photosynthetically active radiation (PAR) <5 mmol $m^{-2} s^{-1}$) as $u^* < 0.10$ m s^{-1}. Data coverage for the growing season was 78.0%, 70.0%, and 82.6% for the D, M, and S sites, respectively.

Table 1 Primary biophysical characteristics of the three study sites: D – inland near the dike, S – a *Scirpus*-dominated submerging site near the sea, and M – a mid-level site between S and D (see Fig. 1)

Site	D	M	S
Dominant species and coverage			
SA	0.715	0.546	0.484
PA	0.254	0.378	0.147
SM	0	0	0.068
Aboveground biomass ($g m^{-2}$)	1170.0 ± 103.1	765.6 ± 82.0	400.7 ± 86.8
Relative elevation (cm)	12	4	0
Distance to the sea (m)	1400	300	0
Soil total C (%)	2.10	1.70	1.50
Soil total N (%)	0.12	0.08	0.06
LAI	4.70	3.84	1.59

Abbreviations for species names: SA, *Spartina alterniflora*; PA, *Phragmites australis*; SM, *Scirpus mariqueter*.

Estimation of GPP. Diel ecosystem respiration was estimated based on an exponential relationship between dark respiration (R) and temperature (T) (Sims *et al.*, 2005):

$$R = R_n \times e^{[k(T_a - T_n)]}, \quad (2)$$

where R_n is the night-time respiration rate, T_n is the mean night-time air temperature corresponding to the data points used to calculate R, and k is the coefficient relating respiration to air temperature (°C) (Fig. 2). GPP is calculated as

$$GPP = R - NEE. \quad (3)$$

The 8-day average GPP and NEE were calculated from the 30 min GPP and NEE to correspond with the temporal interval of MODIS product MOD09A1 (see MODIS data and vegetation indices) for the study period (Fig. 3a–c).

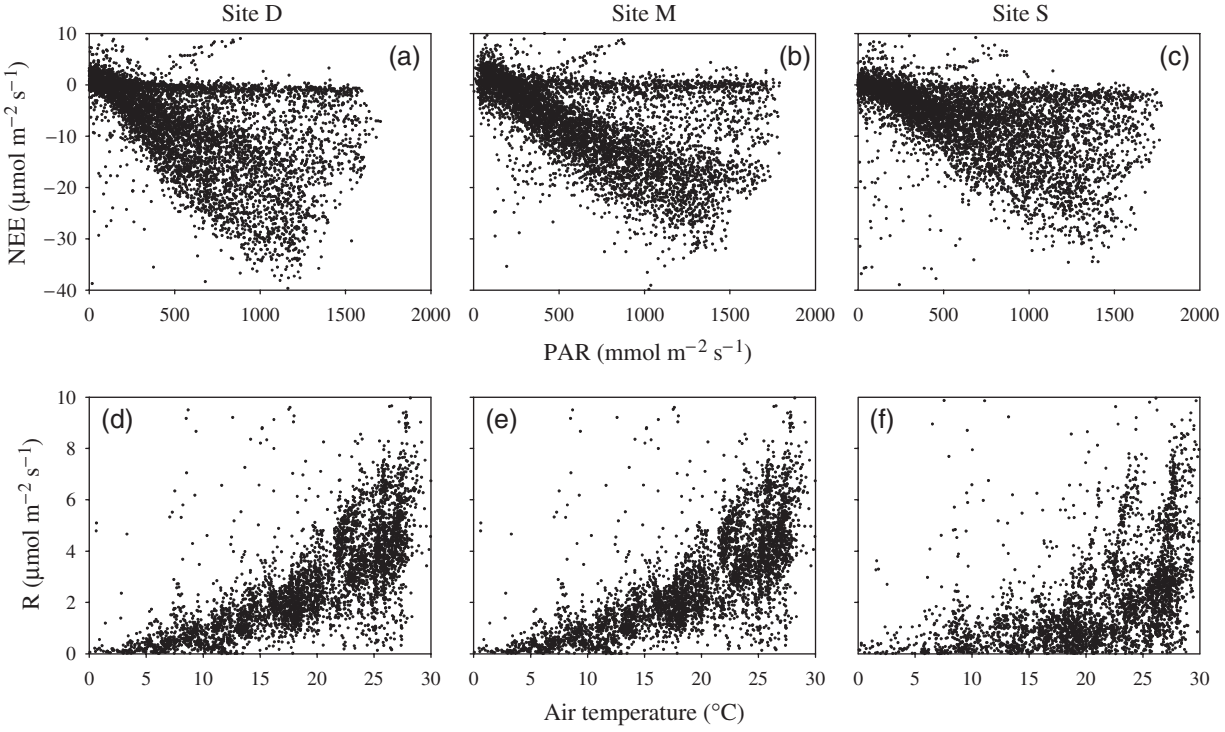

Fig. 2 Changes in daytime net ecosystem exchange (NEE) of CO_2 with photosynthetically active radiation (PAR) (a–c) and nocturnal ecosystem respiration (R) with air temperature (d–f) in the growing season of 2005 (DOY64–DOY320) at the three study sites in the coastal Dongtan wetlands, Shanghai, China.

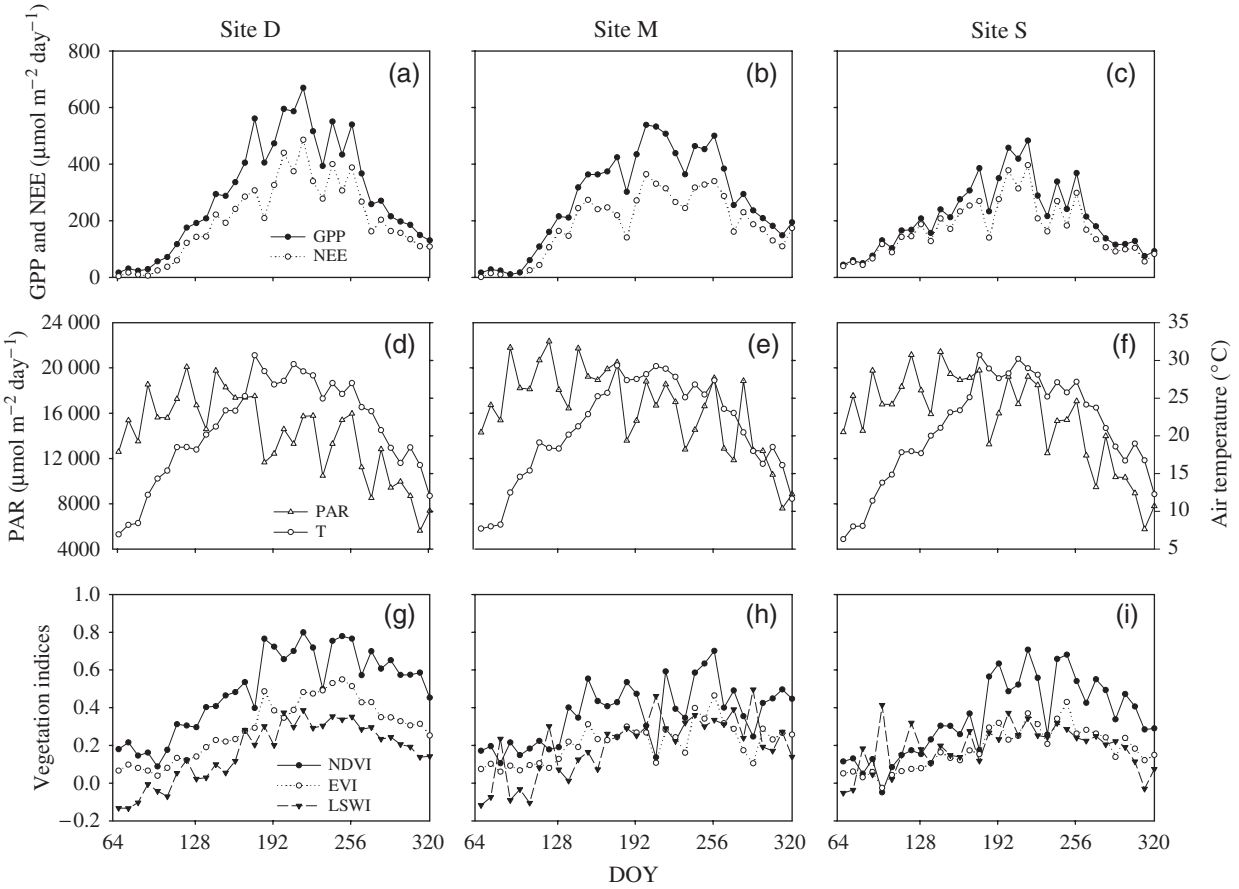

Fig. 3 Seasonal changes in net ecosystem exchange (NEE) of CO_2 and gross primary production (GPP) (a–c); photosynthetically active radiation (PAR) and mean air temperature (*T*) (d–f); and vegetation indices (NDVI, normalized difference vegetation index; EVI, enhanced vegetation index; and LSWI, land surface water index) (g–i) in the 2005 growing season at Dongtan wetlands, Shanghai, China.

Estimation of evapotranspiration. ET was estimated using the methods proposed by Dahm *et al*. (2002). Specifically, meteorological measurements, including mixing ratio, air density, specific heat of air at constant pressure, and latent heat of vaporization of water from the mean water vapor pressure, air temperature, and barometric pressure were used to calculate latent heat fluxes ($W\,m^{-2}$) so that 30 min ET could be determined by dividing the latent heat of vaporization ($4.4\,kJ\,mol^{-1}$). The 8-day average ET was calculated from the 30 min ET corresponding to the same temporal interval of MOD09A1.

MODIS data and vegetation indices

The 8-day composite MODIS product MOD09A1 (500 m spatial resolution) was provided by the University of New Hampshire, which allows the user to retrieve 1 pixel datasets based on geographic location for a specified time span (http://remotesensing.unh.edu/). The latitude and longitude of flux towers were set as centroids of required MODIS pixels. As the 500 m spatial resolution matched the footprint of our flux towers well, we only considered 1 pixel for each site. Data were downloaded from the website, and three indices were calculated for use in models estimating GPP: the normalized difference vegetation index (NDVI), the enhanced vegetation index (EVI), and the land surface water index (LSWI).

To assess the empirical utility of vegetation indices in predicting GPP, we performed correlation analysis between the vegetation indices (NDVI and EVI) and GPP and found that EVI was the best predictor for GPP. LSWI was also included in this study to explore its potential utility for quantifying lateral transportation of carbon related to tidal activities and for modeling CH_4 production. Because we did not have direct measurements of these two fluxes, LSWI was used to quantify the sum of the two terms as the difference between the observed GPP from the EC tower (GPP_{EC}) and predicted GPP from MODIS (GPP_{MODIS}).

Table 2 Empirical coefficients of linear regression analyses estimated based on the Michaelis–Menten model [Eqn (9)] for the three study sites in Dongtan coastal wetlands, Shanghai, China

Site	N	a	GPP_{max}	R^2	F-test
D	720	0.0239	44.2402	0.641	$P<0.05$
M	720	0.0201	39.027	0.605	$P<0.05$
S	1200	0.017	36.6786	0.544	$P<0.05$

Table 3 Comparisons between the observed gross primary production of eddy covariance towers (GPP_{EC}) and model based on MODIS products (GPP_{MODIS}) in the three coastal wetland study sites at Dongtan, Shanghai, China, between DOY36 and DOY321 in 2005

Site	GPP_{EC}	GPP_{MODIS} (RE)
D	295.23	137.48 (53.43%)
M	276.76	102.68 (62.90%)
S	213.36	74.62 (65.03%)

The relative error (RE) was calculated as $RE = [(GPP_{EC} - GPP_{MODIS})/GPP_{EC}] \times 100\%$.

Satellite-based light use efficiency estimation

The LUE model. Xiao *et al*. (2004a) developed a VPM for estimating GPP over the photosynthetically active period of vegetation:

$$GPP = \varepsilon_g \times FPAR_{chl} \times PAR, \quad (4)$$

where $FPAR_{chl}$ is the fraction of PAR absorbed by leaf chlorophyll in the canopy and ε_g is LUE ($\mu mol\, CO_2\, \mu mol^{-1}$), which is affected by temperature, water, and leaf phenology:

$$\varepsilon_g = \varepsilon_0 \times T_{scalar} \times W_{scalar} \times P_{scalar}, \quad (5)$$

where ε_0 is the apparent quantum yield or maximum LUE, and T_{scalar}, W_{scalar}, and P_{scalar} are the scalars for the effects of temperature, water, and leaf phenology on LUE of vegetation, respectively.

Estimations of LUE. ε_0 is largely determined by the choice of either a linear or nonlinear relationship between GPP and absorbed PAR (APAR) over a year (Xiao, 2006). In this study, we first used the Michaelis–Menten (Table 2) function to estimate NEE (Davidson *et al*., 2006):

$$NEE = \frac{\alpha \times APAR \times GPP_{max}}{\alpha \times APAR + GPP_{max}} - R, \quad (6)$$

where R is the ecosystem respiration, and α is the apparent quantum yield or maximum LUE. To estimate ε_g, the parameters for temperature, water, and phenology scalars should first be determined according to Xiao *et al*. (2004a).

$$T_{scalar} = \frac{(T - T_{min})(T - T_{max})}{[(T - T_{min})(T - T_{max})] - (T - T_{opt})^2}, \quad (7)$$

where T_{min}, T_{opt}, and T_{max} are the temperatures and were set to 0, 20, and 35 °C, respectively. In estuarine wetlands, water stress (low water availability) is unlikely to occur, so that W_{scalar} was set to 1.0. P_{scalar} is dependent on the life expectancy of leaves that varies with phenology. For our system, the wetland canopy abounds with foliage in the growing season, and P_{scalar} was set to 1.0.

The integrated model for GPP estimation

The LUE model focuses on C uptake through photosynthesis, while satellite-based GPP estimation depends more on vegetation characteristics (e.g. LAI). GPP_{MODIS} covers neither lateral carbon loss nor CH_4 release (non-CO_2 form). We expected to find some differences between GPP_{EC} and GPP_{MODIS} or ΔGPP (i.e. the magnitude of the lateral carbon flux plus non-CO_2 carbon emissions).

LSWI, ET, TH, and air temperature (T) were selected to evaluate ΔGPP. Because LSWI, ET, and TH are functions of T, T was arbitrarily excluded in the further analysis to reduce bias related to high correlations among the explanatory variables. To reduce the covariance among LSWI, ET, and TH for predicting ΔGPP, we performed principal component analysis (PCA). Additionally, autoregression (AR) analyses between ΔGPP and the three factors (LSWI, ET, and TH) were conducted by using first-order autocorrelated errors to discount the autocorrelations. The following autoregression model was considered with a time-varying autoregressive parameter:

$$\Delta GPP_t = \mu + (\rho + \rho_{t-1})\Delta GPP_{t-1} + \varepsilon_t, \quad (8)$$

where $\varepsilon_t \sim NID\ (0,\ \sigma_\varepsilon^2)$, and ρ_t is a censored latent variable according to Franses *et al*. (2004), defined as

$$\rho = \begin{cases} x_t\beta + \mu_t & \text{if} \quad x_t\beta + \mu_t \geq 0 \\ 0 & \text{if} \quad x_t\beta + \mu_t \leq 0 \end{cases}, \quad (9)$$

where $\mu_t \sim NID\ (0,\ \sigma_\mu^2)$ is independent of ε_t, x_t is a $(K \times 1)$ vector of explanatory variables (TH, ET, and LSWI) including a constant, and β is an unknown $(K \times 1)$ parameter vector.

The final estimation of GPP integrated from the MODIS-derived model and autoregression model is GPP′:

$$GPP' = GPP_{MODIS} + GPP_{REG}. \quad (10)$$

Results

Seasonal changes in NEE and GPP

Both NEE and GPP at three sites exhibited clear seasonal changes corresponding to the changes in physical environment (i.e. temperature, light) and vegetation (Fig. 3), with an initial value near zero between DOY65 and DOY113 (March 4–April 22), when air temperature was below 7 °C (i.e. pregrowing season) regardless of PAR levels (Fig. 3d–f). Vegetation indices also indicated beginning of the growing season during this period. However, we detected a measurable amount of NEE during the same period at Site S where tidal activities were most pronounced (Fig. 3f). As air temperature increased to 10 °C after DOY113, vegetation increased linearly, peaking between DOY170 and DOY260, then decreased until DOY320 (November 8) as temperature and PAR both declined. The *Phragmites*-dominated wetland near the dike (Site D) had the highest peak NEE ($-562.98\,\mu mol\,m^{-2}\,day^{-1}$) and GPP ($669.49\,\mu mol\,m^{-2}\,day^{-1}$) and exhibited the most obvious seasonal pattern. Average values of NEE (GPP) were −202.07 (295.24), −183.87 (276.76), and −170.20 (213.36) $\mu mol\,m^{-2}\,day^{-1}$ for sites D, M, and S, respectively. These figures were consistent with aboveground biomass measured through harvesting the vegetation at peak vegetation growth (Table 1).

Changes in NDVI, EVI, and LSWI with GPP

The vegetation indices derived from MODIS datasets (i.e. NDVI, EVI, and LSWI) captured the dynamics of the vegetation well in 2005 (Fig. 3g and h). All three indices were higher at Sites D and M than at Site S, with an abrupt increase after DOY113 and peaks occurring between DOY200 and DOY260. Biweekly fluctuations in NDVI, EVI, and LSWI occurred at the same pace with tidal changes and were more pronounced at Sites S and M (both were closer to the ocean) than at Site D. The mean NDVI (EVI) values for sites D, M, and S were 0.498 (0.293), 0.370 (0.212), and 0.351 (0.182), respectively, while the mean LSWI values were 0.165, 0.197, and 0.190, respectively. The seasonal dynamics of EVI differed from NDVI in magnitude during the middle of the growing season. The maximum NDVI values ranged between 0.70 and 0.80 and were much higher than the maximum EVI (0.43–0.55). NDVI reached and maintained its maximum level at Site D after DOY193, but not at other sites. Interestingly, none of the indices reached their pregrowing season levels from DOY65, suggesting a continuous decrease over the winter months. The correlations between the vegetation indices and GPP were significantly different among the three sites (Fig. 4), with strong correlations found at both sites D and S, but poor correlations at Site M. EVI displayed a stronger linear relationship with GPP than did NDVI (Fig. 4).

Predicting GPP from the LUE model

The LUE model was run at an 8-day time scale using site-specific temperature, PAR, and vegetation indices for the study period. Predicted GPP (GPP_{MODIS}) did not match the observed GPP (GPP_{EC}) well (Fig. 5). GPP_{MODIS} was lower than GPP_{EC}, except for two 8-day periods at Site M early in the growing season. Daily average GPP_{MODIS} from March to November accounted for 53.4% to 65.0% of GPP_{EC}, with the discrepancy increasing from Site D to Site S (Table 3). The difference (i.e. GPP) between GPP_{EC} and GPP_{MODIS} suggested that significant lateral movement of carbon and CH_4 emission might have occurred.

Factors regulating GPP

The correlation analysis between ΔGPP and LSWI, ET, and TH suggested strong influences of tides and vegetation (Table 4) at all three sites. The two inland sites (D and M) showed stronger correlations between ΔGPP and TH ($R^2 = 0.86$ and 0.90, respectively) than did Site S ($R^2 = 0.74$), located at the submerging zone and frequently affected by tides. LSWI and ET showed similar correlations with ΔGPP for the three sites.

The PCA indicated that one principal component, which had an eigenvalue >1, explained 83.31% of the variance, and was negatively correlated with TH (−0.938), LSWI (−0.879), and ET (−0.921) (Table 5). Further analysis based on autoregression procedures with first-order autocorrelated errors showed that the standard error of the estimate was 58.691 when all three variables (TH, LSWI, and ET) were considered, with LSWI behaving as a non-significant variable ($P = 0.106$). Consequently, we developed a new autoregression model with TH and ET as independent variables to predict ΔGPP (Table 6), so that actual GPP′ could be calculated using [Eqn (10)].

GPP′ estimation

The underestimated GPP based on MODIS was obvious when compared to the tower-based estimates (Fig. 5). GPP′ appeared to be lower than GPP_{EC} in summer, but higher in the spring and late growing season (Fig. 5a–c). Our final models for the three study sites accounted, on average, for 87.6% ($R^2 = 0.876$) of the variation in the data, with a range of 91.8% (Site D) to 71.66% (Site S). The accuracy of the GPP estimates increased by 32.6%,

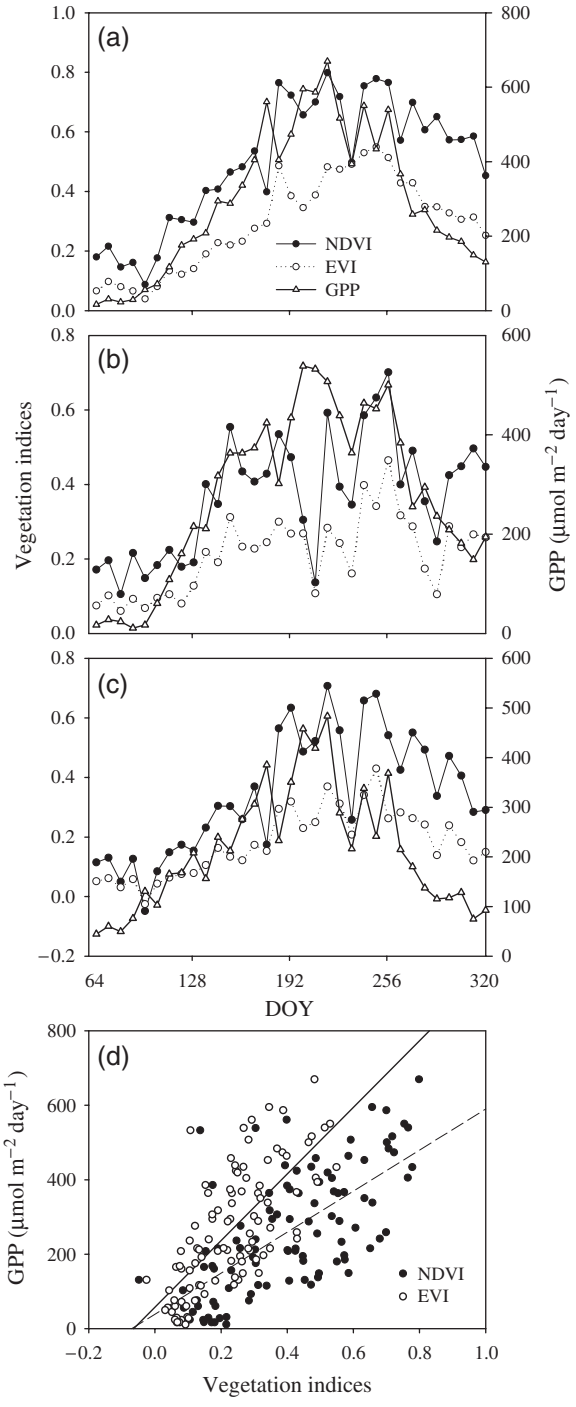

Fig. 4 Comparisons between vegetation indices (EVI, NDVI) and gross primary production (GPP) among three sites at Dongtan, China (a, Site D; b, Site M; c, Site S). Simple linear regression models between GPP and vegetation (NDVI, EVI) are shown with data combined from all three sites (d). The solid line represents the relationship between GPP and EVI (GPP = 894.18EVI + 57.826, $R^2 = 0.5203$) and the dashed line between GPP and NDVI (GPP = 550.81DVI + 38.768, $R^2 = 0.4601$).

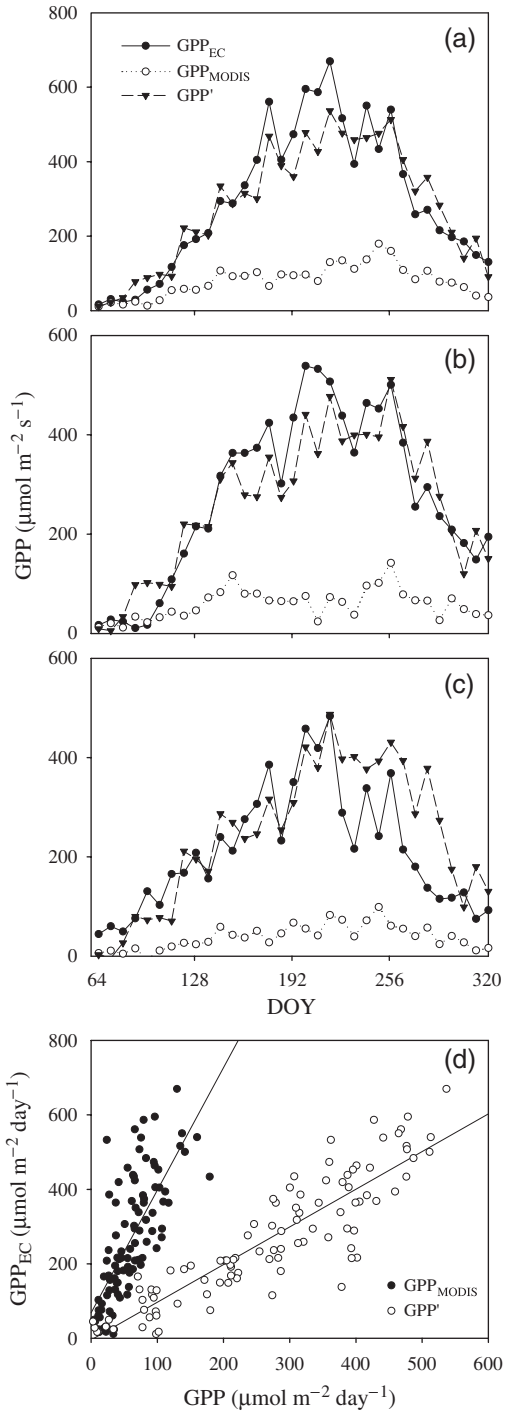

Fig. 5 Comparisons of seasonal changes in gross primary production from eddy covariance towers (GPP_{EC}), the MODIS-based model (GPP_{MODIS}), and the hybrid model (GPP′) Eqn (13) for the 2005 growing season at three sites (a, Site D; b, Site M; c, Site S). Simple linear relationships between GPP_{EC}, GPP_{MODIS}, and GPP′ are presented with data combined from all three sites ($GPP_{EC} = 3.29 \times GPP_{MODIS} + 68.133$, $R^2 = 0.550$; $GPP_{EC} = 1.025 \times GPP' - 6.18$, $R^2 = 0.876$) (d).

on average, ranging from 23.5% at Site S to 42.9% at Site M.

Discussion and summary

Wetlands represent the largest component of the terrestrial biological carbon pool, and thus play an important role in the global carbon cycle (Chmura *et al*., 2003). However, relatively few studies on carbon flux have been conducted in coastal wetlands from an ecosystem perspective compared to those in terrestrial ecosystems. First, acquiring ground data in these ecosystems is extremely costly both in time and labor due to access difficulties (Smith *et al*., 1998). Second, there is a distinct lack of long-term observations in these systems (http://www-eosdis.oml.gov/fluxnet/). Our establishment of carbon flux towers at Dongtan is a pioneering effort to permanently measure carbon flux in coastal wetlands. Because tidal dynamics affect water level and other physical features, coastal wetlands encompass complex hydrological environments. Accordingly, estimating ecosystem production (e.g. GPP) of coastal wetlands is challenging because of the significant amount of carbon (dissolved and organic materials) carried by sea waves, as well as CH_4 emission that is not measured by conventional EC techniques (i.e. CO_2 only). Two models, the LUE model and an integrated model introduced in this study, were used to evaluate the biophysical performance of GPP. The quantitative relationships between the vegetation indices and carbon flux data in our study area demonstrated the needs to improve LUE model with EVI in terms of the magnitude of photosynthesis. Our integrated model used a combination of autoregression analysis and comparisons of the differences between direct observations and estimates obtained from a model based on satellite imagery (i.e. LUE) to estimate GPP for three estuarine wetlands along a gradient from the sea to inland at Dongtan of Chongming Island, Shanghai, China. Unlike previous studies in non-wetland ecosystems, the predicted GPP from the LUE model (GPP_{MODIS}) underestimated GPP relative to that observed from eddy flux tower measurements (GPP_{EC}) ($R^2 = 0.47$–0.65) for our sites. We attributed this underestimation to lateral carbon flux caused by tides and to emission of carbon in non-CO_2 form (i.e. CH_4). Both these processes are prevalent in coastal wetland ecosystems but are not captured by the existing MODIS–LUE model.

Vegetation measurements from MODIS data provide an indirect approach to predicting the differences between the simulated and measured GPP. Our results (Fig. 5; Table 3) indicated that tidal activities, land surface water content (LSWI), and vegetation indices correlated strongly with carbon fluxes measured at the EC towers. Our autoregression analysis [Eqn (13)] successfully identified tidal height and ET as the most important variables predicting the differences between the two GPP estimates, thus accounting for lateral carbon movement and CH_4 emission and allowing us to calculate actual production (i.e. GPP′). Predictions based on autoregression models showed substantial improvement in the accuracy of GPP estimation (R^2 increased from 0.55 to 0.87) (Fig. 5).

Estimating carbon flux in coastal wetlands is a persistent challenge, especially in the context of global warming, because these ecosystems are very sensitive to changes in water level or climate (Chimner & Cooper, 2003; Weltzin *et al*., 2003), which will also likely result in changes to freshwater inputs and timing for coastal wetlands. Sea level rise and increasingly common extreme weather events may modify the hydrology and vegetation cover in coastal regions, potentially inducing changes in carbon cycles through increasing the depth or time of inundation or through decreasing the quantity of sediments, and therefore nutrients, deposited (http://ipcc-wg1.ucar.edu/wg1/wg1-report.html). For example, Chimner & Cooper (2003) reported mean CO_2 emissions of $453.7\,mg\,CO_2\text{-}C\,m^{-2}\,h^{-1}$ when the water table was between 0 and 5 cm below the soil surface, but when the water table increased to 1–5 cm above the soil surface, mean CO_2 emissions decreased to $231.3\,mg\,CO_2\text{-}C\,m^{-2}\,h^{-1}$. It has been reported that the relative sea level of the Yangtze River Delta could rise 25–50 cm by the year 2050, resulting in important consequences for the carbon cycle of the region (Shi *et al*., 2000). Therefore, integrating classical models such

Table 4 Correlation coefficients of ΔGPP with the land surface water index (LSWI), evapotranspiration (ET), and tide height (TH) at the three coastal wetland study sites at Dongtan, Shanghai, China

Site	TH	LSWI	ET
D	0.86	0.80	0.95
M	0.90	0.70	0.82
S	0.74	0.57	0.61
Mean	0.82	0.70	0.80

All correlation coefficients are significant at $P < 0.05$.

Table 5 Results of a principal component analysis (PCA) incorporating the land surface water index (LSWI), evapotranspiration (ET), and tidal height (TH)

Component	Eigenvalue	Variance explained (%)	Eigenvectors		
			TH	LSWI	ET
PCA 1	2.50	83.31	−0.938	−0.879	−0.921
PCA 2	0.33	11.16	0.157	−0.474	0.292
PCA 3	0.17	5.52	0.308	−0.058	−0.259

Table 6 Estimated coefficients and statistics for two autoregression (AR) models developed to predict ΔGPP from the land surface water index (LSWI), evapotranspiration (ET), and tide height (TH) at the three study sites

	Unstandardized coefficients		Standardized coefficients		
	B	SE	*β*	*T*	Significance
Model 1					
TH	3.872	1.112	0.306	3.484	0.001
LSWI	88.524	54.194	0.131	1.633	0.106
ET	0.220	0.046	0.415	4.729	0.000
(Constant)	−801.378	231.017		−3.469	0.001
Model 2					
TH	4.076	1.103	0.323	3.695	0.000
ET	0.231	0.046	0.440	5.028	0.000
(Constant)	−837.567	230.212		−3.638	0.000

The Prais–Winsten estimation method is used in AR model development. The mean and standard deviation of Rho in Model 1 were 0.683 and 0.075, respectively (Franses *et al*., 2004).

as LUE and autoregression model, that take into account the unique properties of coastal ecosystems, can provide a way to more accurately keep abreast of important changes to the carbon cycles of coastal wetlands.

The effect of ET on CH_4 release in wetland ecosystems (e.g. *Phragmites australis*) is well documented. Grunfeld & Brix (1999) reported that 62% of midday CH_4 emission from vegetated sediments occurred through the internal gas-spaces of plants and that transpiration-induced transport of alternative electron acceptors into the sediments can also contribute to higher CH_4 oxidation in vegetated sediments. ET, a major parameter considered in our study, is an important proxy for the effect of increasing the internal gas-spaces. A large part (37.8%) of the plant community at Site M consisted of *Phragmites* sp. (Table 1). Our integrated model improved predictions of GPP at Site M by 42.9%, while substantial improvements at Site D (27.1%) and Site S (23.5%) were also achieved (Table 1). These results may partially reflect the importance of ET to CH_4 emission. Though the predicted GPP for Site S from the integrated model improved somewhat, the improvement was relatively limited compared to improvements for Sites D and M. We attribute this to the lower vegetation density at Site S. The aboveground plant biomass at this site was the lowest among the three sites (Table 1), resulting in less plant litter and a reduction in the effect of evaporation and/or tidal height (Table 4).

To more fully examine the influence of the vegetation indices, we analyzed the relationships between the indices and TH (Table 7). Our results showed negative correlations between the vegetation indices and TH because the addition of water surface results in lower reflectance of the near-infrared wavelength. The tide effect amplified the bias in EVI measurement by

Table 7 Correlation coefficients (*R*) of tidal height (TH) with the normalized difference vegetation index (NDVI) and enhanced vegetation index (EVI) at the three study sites

Site	NDVI	EVI
D	−0.05	−0.08
M	−0.04	−0.07
S	−0.11	−0.18

All correlation coefficients were significant at $P<0.05$. The mean TH values during MODIS overpass were used.

MODIS, leading to inaccuracy in MODIS-derived GPP estimation. Figure 3 shows some clear sinking points of EVI and NDVI in summer, especially at Site S near the sea. In the Dongtan area, the average TH is significantly higher in summer than in other seasons, and the higher water level affects the measurement of the light spectrum. Compared with upland ecosystems (Xiao *et al*., 2004a, 2005), however, the correlations between the vegetation indices and GPP are low because of more complex dynamics in wetland ecosystems (e.g. water in tidal areas). Therefore, accurately estimating TH is a key to improving the vegetation indices and forecasts of the lateral carbon flow in coastal areas. Fortunately, with the development of remote-sensing techniques, mapping tidal height is possible. Satellite microwave sensors, such as the Radar Altimeter, Microwave Scatterometer and SAS (synthetic aperture radar), can detect sea level and sea wave height. High-frequency (HF) radars can detect tidal circulation patterns and estuarine outflow plumes in a large region with sufficient spatial resolution (Marmorino *et al*., 2004; Sentchev *et al*., 2006). By using phased-array HF radars, Haus *et al*. (2006) measured the near-surface current

velocities and wave heights near the mouth of the Chesapeake Bay in 1997, finding good agreement with results obtained from direct measurement. Once we obtain the tidal height from the high spatial resolution remote-sensing data, we can predict lateral carbon flow over a broader area by integrating TH, ground-based measurements of lateral carbon flow, and carbon circulation models.

We have focused on TH and ET in this study as the most important variables for predicting the differences between GPP_{EC} and GPP_{MODIS}. However, there are other potential factors that may also influence the lateral flow of carbon and CH_4 emission, such as climate, sea temperature and salinity, soil physical and biological variables, depth of the methane oxidizing horizon (Potter, 1997) and the extent of 'outwelling,' marsh productivity and vegetation coverage, tidal amplitude, and geomorphology (Odum, 2000). Future studies are needed to examine these variables. It is well known that regional CH_4 estimation is very important for understanding the ecosystem carbon cycle, but biogeochemical models concerning CH_4 estimation in coastal wetlands have been few because appropriate methods to estimate the effect of water table fluctuations on carbon cycles are yet to be discovered. Although CH_4 emissions in forested wetlands have been simulated successfully by Wetland-DNDC, a model derived from PnET-N-DNDC (Cui *et al*., 2005a, b), tidal activities must be considered if the model is applied to coastal wetlands. However, with the help of remote-sensing techniques, especially the high spectral remote sensing AVIRIS (Airborne Visible Infrared Imaging Spectrometer), we can improve our understanding of the regional methane flux (Leifer *et al*., 2006). The launch of SCIAMACHY (Scanning Imaging Absorption Spectrometer for Atmospheric Chartography) provides us with a new tool for analyzing the biogeochemical cycle of methane, and its feasibility has been verified (Frankenberg *et al*., 2005, 2006; Bergamaschi *et al*., 2007). Further analyses on the relationships between CH_4 emission and the related variables derived from remote-sensing images will likely become the reality in the near future.

In summary, we have simulated the seasonal dynamics of GPP for three sites in the estuarine wetland ecosystem at Dongtan using the LUE model, and also by combining the LUE model with *in situ* measurements of climate data and MODIS vegetation indices, using net CO_2 exchange data for parameter estimation. Predicted GPP from the LUE model did not agree well with observed GPP from the eddy flux towers (R^2 ranging from 0.47 to 0.64), with substantial differences among the three sites. We hypothesized that the differences were due to lateral carbon flow related to tidal activities and vertical CH_4 emissions that are not accounted for by EC measurements. To estimate GPP more accurately for this estuarine wetland ecosystem, we conducted autoregression analyses to identify significant variables (i.e. ET, TH) capable of predicting the difference between GPP_{EC} and GPP_{MODIS}. Ground-based measurements of lateral carbon flow and CH_4 emission are needed to validate our models before they can be applied to predicting GPP of other coastal wetlands.

Acknowledgements

This research was supported by the National Basic Research Program of China (Grant no. 2006CB403305), the National Natural Science Foundation of China (no. 40471087), Shanghai Municipal Natural Science Foundation (no. 06zr14015), the Program for New Century Excellent Talents in University (NCET) through the Ministry of Education of China, and the US–China Carbon Consortium (USCCC). We thank Chongming Dongtan National Natural Reserve and the students in our laboratories for their assistance in constructing the flux towers and for assisting with other field research. Dr Kim Brosofske provided careful editing of an earlier version of the manuscript.

References

Baldocchi D, Falge E, Wilson K (2001) A spectral analysis of biosphere–atmosphere trace gas flux densities and meteorological variables across hour to multi-year time scales. *Agricultural & Forest Meteorology*, **107**, 1–27.

Bange HW (2006) Nitrous oxide and methane in European coastal waters. *Estuarine Coastal & Shelf Science*, **70**, 361–374.

Bergamaschi P, Frankenberg C, Meirink JF *et al*. (2007) Satellite chartography of atmospheric methane from SCIAMACHY on board ENVISAT: 2. Evaluation based on inverse model simulations. *Journal of Geophysical Research – Atmospheres*, **112**, D02304, doi: 10.1029/2006JD007268.

Boegh E, Soegaard H (2004) Remote sensing based estimation of evapotranspiration rates. *International Journal of Remote Sensing*, **25**, 2535–2551.

Chen G, Chen Y (2004) Some aspects of spatial aliasing in satellite altimetry. *International Journal of Remote Sensing*, **25**, 5525–5535.

Chen J, Saunders SC, Brosofske KD, Crow TR (eds) (2006) *Ecology of Hierarchical Landscapes: from Theory to Application*. Nova Science Publisher, New York, USA.

Chimner RA, Cooper DJ (2003) Influence of water table levels on CO_2 emissions in a Colorado subalpine fen: an in situ microcosm study. *Soil Biology & Biochemistry*, **35**, 345–351.

Chmura GL, Anisfeld SC, Cahoon DR, Lynch JC (2003) Global carbon sequestration in tidal, saline wetland soils. *Global Biogeochemical Cycles*, **17**, 1111–1123.

Cui JB, Li CS, Trettin C (2005a) Analyzing the ecosystem carbon and hydrologic characteristics of forested wetland using a biogeochemical process model. *Global Change Biology*, **11**, 278–289.

Cui JB, Li CS, Trettin C (2005b) Modeling biogeochemistry and forest management practices for assessing GHGs mitigation strategies in forested wetlands. *Environmental Modeling & Assessment*, **10**, 43–53.

Dahm CN, Cleverly JR, Coonrod JEA, Thibault JR, McDonnell DE, Gilroy DF (2002) Evapotranspiration at the land/water interface in a semi-arid drainage basin. *Freshwater Biology*, **47**, 831–843.

Davidson EA, Janssens IA, Luo YQ (2006) On the variability of respiration in terrestrial ecosystems: moving beyond Q_{10}. *Global Change Biology*, **12**, 154–164.

Drake BG, Muehe MS, Peresta G, GonzalezMeler MA, Matamala R (1996) Acclimation of photosynthesis, respiration and ecosystem carbon flux of a wetland on Chesapeake Bay, Maryland to elevated atmospheric CO_2 concentration. *Plant and Soil*, **187**, 111–118.

Duan XN, Wang XK, Mu YJ, Ouyang ZY (2005) Seasonal and diurnal variations in methane emissions from Wuliangsu Lake in arid regions of China. *Atmospheric Environment*, **39**, 4479–4487.

Frankenberg C, Meirink JF, Bergamaschi P *et al*. (2006) Satellite chartography of atmospheric methane from SCIAMACHY on board ENVISAT: analysis of the years 2003 and 2004. *Journal of Geophysical Research – Atmospheres*, **111**, D07303, doi: 10.1029/2005JD006235.

Frankenberg C, Meirink JF, van Weele M, Platt U, Wagner T (2005) Assessing methane emissions from global space-borne observations. *Science*, **308**, 1010–1014.

Franses PH, Paap R, Vroomen B (2004) Forecasting unemployment using an autoregression with censored latent effects parameters. *International Journal of Forecasting*, **20**, 255–271.

Gebremichael M, Barros AP (2006) Evaluation of MODIS gross primary productivity (GPP) in tropical monsoon regions. *Remote Sensing of Environment*, **100**, 150–166.

Grunfeld S, Brix H (1999) Methanogenesis and methane emissions: effects of water table, substrate type and presence of *Phragmites australis*. *Aquatic Botany*, **64**, 63–75.

Haus BK, Ramos RJ, Graber HC, Shay LK, Hallock ZR (2006) Remote observation of the spatial variability of surface waves interacting with an estuarine outflow. *IEEE Journal of Oceanic Engineering*, **31**, 835–849.

Heinsch FA, Zhao MS, Running SW *et al*. (2006) Evaluation of remote sensing based terrestrial productivity from MODIS using regional tower eddy flux network observations. *IEEE Transactions on Geoscience & Remote Sensing*, **44**, 1908–1925.

Houborg RM, Soegaard H (2004) Regional simulation of ecosystem CO_2 and water vapor exchange for agricultural land using NOAA AVHRR and Terra MODIS satellite data. Application to Zealand, Denmark. *Remote Sensing of Environment*, **93**, 150–167.

Hughes CE, Binning P, Willgoose GR (1998) Characterisation of the hydrology of an estuarine wetland. *Journal of Hydrology*, **211**, 34–49.

Leifer I, Roberts D, Margolis J, Kinnaman F (2006) In situ sensing of methane emissions from natural marine hydrocarbon seeps: a potential remote sensing technology. *Earth & Planetary Science Letters*, **245**, 509–522.

Leuning R, Cleugh HA, Zegelin SJ, Hughes D (2005) Carbon and water fluxes over a temperate Eucalyptus forest and a tropical wet/dry savanna in Australia: measurements and comparison with MODIS remote sensing estimates. *Agricultural & Forest Meteorology*, **129**, 151–173.

Leuning R, Moncrieff J (1990) Eddy-covariance CO_2 flux measurements using open-path and closed-path CO_2 analyzers – corrections for analyzer water-vapor sensitivity and damping of fluctuations in air sampling tubes. *Boundary-Layer Meteorology*, **53**, 63–76.

Li ZQ, Yu GR, Li QK, Fu YL, Li YN (2006) Effect of spatial variation on areal evapotranspiration simulation in Haibei, Tibet plateau, China. *International Journal of Remote Sensing*, **27**, 3487–3498.

Marmorino GO, Shen CY, Evans TE, Lindemann GJ, Hallock ZR, Shay LK (2004) Use of 'velocity projection' to estimate the variation of sea-surface height from HF Doppler radar current measurements. *Continental Shelf Research*, **24**, 353–374.

Martinelli LA, Devol AH, Victoria RL, Richey JE (1991) Stable carbon isotopic variation in C3 and C4 plants along the Amazon River. *Nature*, **353**, 57–59.

Nagler PL, Cleverly J, Glenn E, Lampkin D, Huete A, Wan Z (2005a) Predicting riparian evapotranspiration from MODIS vegetation indices and meteorological data. *Remote Sensing of Environment*, **94**, 17–30.

Nagler PL, Scott RL, Westenburg C, Cleverly JR, Glenn EP, Huete AR (2005b) Evapotranspiration on western US rivers estimated using the Enhanced Vegetation Index from MODIS and data from eddy covariance and Bowen ratio flux towers. *Remote Sensing of Environment*, **97**, 337–351.

Odum EP (1968) A research challenge: evaluating the productivity of coastal and estuarine water. In: *Proceedings of the Second Sea Grant Congress*. University of Rhode Island, Rhode Island, USA, pp. 63–64.

Odum EP (2000) Tidal marshes as upwelling/pulsing systems. In: *Concepts and Controversies in Tidal Marsh Ecology* (eds Weinstein MP, Kreeger DA), pp. 3–7. Kluwer Academic Publishers, Dordrecht, the Netherlands.

Paw U KT, Baldocchi DD, Meyers TP, Wilson KB (2000) Correction of eddy-covariance measurements incorporating both advective effects and density fluxes. *Boundary-Layer Meteorology*, **97**, 487–511.

Potter CS (1997) An ecosystem simulation model for methane production and emission from wetlands. *Global Biogeochemical Cycles*, **11**, 495–506.

Reich PB, Turner DP, Bolstad P (1999) An approach to spatially distributed modeling of net primary production (NPP) at the landscape scale and its application in validation of EOS NPP products. *Remote Sensing of Environment*, **70**, 69–81.

Running SW, Baldocchi DD, Turner DP, Gower ST, Bakwin PS, Hibbard KA (1999) A global terrestrial monitoring network integrating tower fluxes, flask sampling, ecosystem modeling and EOS satellite data. *Remote Sensing of Environment*, **70**, 108–127.

Scanlon TM, Albertson JD (2003) Water availability and the spatial complexity of CO_2, water, and energy fluxes over a heterogeneous sparse canopy. *Journal of Hydrometeorology*, **4**, 798–809.

Sentchev A, Yaremchuk M, Lyard F (2006) Residual circulation in the English Channel as a dynamically consistent synthesis of shore-based observations of sea level and currents. *Continental Shelf Research*, **26**, 1884–1904.

Shi YF, Zhu JW, Xie ZR, Ji ZX, Jiang ZX, Yang GS (2000) Prediction and prevention of the impacts of sea level rise on the Yangtze River Delta and its adjacent areas. *Science in China Series D – Earth Sciences*, **43**, 412–422.

Sims DA, Rahman AF, Cordova VD *et al*. (2005) Midday values of gross CO_2 flux and light use efficiency during satellite overpasses can be used to directly estimate eight-day mean flux. *Agricultural & Forest Meteorology*, **131**, 1–12.

Smith GM, Spencer T, Murray AL, French JR (1998) Assessing seasonal vegetation change in coastal wetlands with airborne remote sensing: an outline methodology. *Mangroves & Salt Marshes*, **2**, 15–28.

Teal JM (1962) Energy flow in the salt marsh ecosystem of Georgia. *Ecology*, **43**, 614–624.

Turner DP, Ritts WD, Cohen WB *et al*. (2003a) Scaling Gross Primary Production (GPP) over boreal and deciduous forest landscapes in support of MODIS GPP product validation. *Remote Sensing of Environment*, **88**, 256–270.

Turner DP, Ritts WD, Cohen WB *et al*. (2005) Site-level evaluation of satellite-based global terrestrial gross primary production and net primary production monitoring. *Global Change Biology*, **11**, 666–684.

Turner DP, Ritts WD, Zhao M *et al*. (2006) Assessing interannual variation in MODIS-based estimates of gross primary production. *IEEE Transactions on Geoscience & Remote Sensing*, **44**, 1899–1907.

Turner DP, Urbanski S, Bremer D, Wofsy SC, Meyers T, Gower ST, Gregory M (2003b) A cross-biome comparison of daily light use efficiency for gross primary production. *Global Change Biology*, **9**, 383–395.

Waring RH, Law BE, Goulden ML, Bassow SL, McCreight RW, Wofsy SC, Bazzaz FA (1995) Scaling gross ecosystem production at Harvard Forest with remote-sensing – a comparison of estimates from a constrained Quantum-Use Efficiency Model and eddy-correlation. *Plant, Cell and Environment*, **18**, 1201–1213.

Weltzin JF, Bridgham SD, Pastor J, Chen J, Harth C (2003) Potential effects of warming and drying on peatland plant community composition. *Global Change Biology*, **9**, 141–151.

Winter P, Schlacher T, Baird D (1996) Carbon flux between an estuary and the ocean: a case for outwelling. *Hydrobiologia*, **337**, 123–132.

Xiao X (2006) Light absorption by leaf chlorophyII and maximun light use efficiency. *IEEE Transactions on Geoscience & Remote Sensing*, **44**, 1933–1935.

Xiao XM, Hollinger D, Aber J, Goltz M, Davidson EA, Zhang QY, Moore B (2004a) Satellite-based modeling of gross primary production in an evergreen needleleaf forest. *Remote Sensing of Environment*, **89**, 519–534.

Xiao XM, Zhang QY, Braswell B *et al*. (2004b) Modeling gross primary production of temperate deciduous broadleaf forest using satellite images and climate data. *Remote Sensing of Environment*, **91**, 256–270.

Xiao XM, Zhang QY, Saleska S *et al*. (2005) Satellite-based modeling of gross primary production in a seasonally moist tropical evergreen forest. *Remote Sensing of Environment*, **94**, 105–122.